

Article

Effect of Segregation on Deformation Behaviour of Nanoscale CoCrCuFeNi High-Entropy Alloy

Arseny M. Kazakov ¹, Azat V. Yakhin ¹, Elvir Z. Karimov ², Rita I. Babicheva ³, Andrey A. Kistanov ¹
and Elena A. Korznikova ^{1,*}

¹ The Laboratory of Metals and Alloys under Extreme Impacts, Ufa University of Science and Technology, 450076 Ufa, Russia; arseny.m.kazakov@gmail.com (A.M.K.)

² Skobeltsyn Institute of Nuclear Physics, Lomonosov Moscow State University, 119991 Moscow, Russia

³ School of Mechanical and Aerospace Engineering, Nanyang Technological University, Singapore 639798, Singapore

* Correspondence: elena.a.korznikova@gmail.com

Abstract: A molecular dynamics (MD) simulation method is used to investigate the effect of grain boundary (GB) segregation on the deformation behavior of bicrystals of equiatomic nanoscale CoCrCuFeNi high-entropy alloy (HEA). The deformation mechanisms during shear and tensile deformation at 300 K and 100 K are analyzed. It is revealed that upon tensile deformation, the stacking fault formation, and twinning are the main deformation mechanisms, while for the shear deformation, the main contribution to the plastic flow is realized through the GB migration. The presence of the segregation at GBs leads to the stabilization of GBs, while during the shear deformation of the nanoscale CoCrCuFeNi HEA without the segregation at GBs, GBs are subject to migration. It is found that the GB segregation can differently influence the plasticity of the nanoscale CoCrCuFeNi HEA, depending on the elemental composition of the segregation layer. In the case of copper and nickel segregations, an increase in the segregation layer size enhances the plasticity of the nanoscale CoCrCuFeNi HEA. However, an increase in the thickness of chromium segregations deteriorates the plasticity while enhancing maximum shear stress. The results obtained in this study shed light on the development of HEAs with enhanced mechanical properties via GB engineering.

Keywords: high-entropy alloys; molecular dynamics; cryogenic temperatures; grain boundary segregation; shear deformation; stretching



Citation: Kazakov, A.M.; Yakhin, A.V.; Karimov, E.Z.; Babicheva, R.I.; Kistanov, A.A.; Korznikova, E.A. Effect of Segregation on Deformation Behaviour of Nanoscale CoCrCuFeNi High-Entropy Alloy. *Appl. Sci.* **2023**, *13*, 4013. <https://doi.org/10.3390/app13064013>

Academic Editor: Theodore E. Matikas

Received: 26 February 2023

Revised: 19 March 2023

Accepted: 20 March 2023

Published: 21 March 2023



Copyright: © 2023 by the authors. Licensee MDPI, Basel, Switzerland. This article is an open access article distributed under the terms and conditions of the Creative Commons Attribution (CC BY) license (<https://creativecommons.org/licenses/by/4.0/>).

1. Introduction

The development of modern technologies applies high standards to the characteristic and properties of new materials. In that sense, traditional metals are inferior to modern alloys in several characteristics. For example, aluminum-based alloys and austenitic steel are potential materials for use in cryogenic temperature applications. However, their main drawback is the insufficient fracture toughness and associated high brittleness at low temperatures [1,2]. Therefore, there is a need to search for advanced materials for applications at cryogenic temperatures. In this regard, high-entropy alloys (HEA), which are formed by mixing four or more elements, are actively being studied. Due to their unique characteristics, such as high specific entropy, slow diffusion, and strong lattice distortion [3], they demonstrate enhanced mechanical and physical properties [4] compared to traditional metals, which corresponds to the current demand of modern production. HEAs provide a vast design space for the creation of new compositions, leading to endless possibilities for novel materials with unique properties. Different combinations of elements to develop new HEAs with tailored characteristics are actively being explored revealing to have multifunctional properties such as catalytic activity, magnetic properties, and thermal stability. This provides possibilities for new applications in diverse fields such as energy storage, sensors, and biomedical devices.

The CoCrFeMnNi alloy, also called the Cantor alloy, is one of the most common HEAs [5]. One of the methods to obtain HEAs is casting, i.e., pouring molten metal into an empty-shaped space. However, since HEAs contain many elements, it is necessary to carry out several melts and control various process parameters. In addition to the casting method, vacuum arc melting [6–9], pressing [10], and laser cladding [11] can be recalled as common approaches of HEA production. Nevertheless, in addition to experimental studies [12,13] great efforts in the study of the mechanical and physical properties of HEAs are carried out by simulation methods, including first-principles [14] and molecular dynamics (MD) [15] approaches. In some cases, first-principles calculations can be an excellent approach to predict the experimental behavior of HEAs. Consideration of numerous correlation methods allows researchers to investigate an extensive range of physical properties of materials. First-principles calculations can be applied in completely different areas, from mineralogy [16] to vibrational spectroscopy [17]. Ab initio modelling can also be a very powerful tool for the design of materials. Instead of being just descriptive, the method allows analyzing and predicting material properties on an atomistic scale.

Experimental studies of HEAs are often time-consuming and costly; therefore, computational methods are crucial tools for analyzing and predicting the material behavior to facilitate an experimental study [18,19]. For instance, first-principles-based simulations can be used to study phase formation, diffusion, Gibbs free energy, excess entropy, and linear thermal expansion coefficient [20]. These results demonstrate high reliability and accuracy comparable to the experiment [21,22]. Structure evolution is often studied experimentally using differential scanning calorimetry, a scanning electron microscope, and an electron probe microanalyzer, and these results match well with those predicted based on first-principles calculations [23]. However, the ability of the ab initio method for the deep investigation of crystal lattice properties is usually limited by the size of the computational cell. This, in fact, eliminates the possibility of studying lattice defects in crystalline materials, except for vacancies and interstitial atoms. At the same time, other defect types, such as dislocations and grain boundaries, make an important contribution to the properties of HEAs and dictate their deformation behavior. This forces researchers to search for simulation methods capable of simulating crystals of a larger volume.

MD simulations are a well-known approach for the modelling of metals and alloys. This method often provides results that are in good agreement with both experimental data and first-principles calculations [24], while it is less time-consuming and computationally costly. MD simulations allow considering larger time and dimension scales when compared to first-principles simulations. This approach is becoming increasingly popular because it is an effective tool for studying crystal structure evolution under the influence of various internal and external factors, for example, for studying crowdions [25–28], the thermal stability of carbon nanomaterials [29–31], phase transitions [32], and electromagnetic effects in crystals [33].

Various properties of HEAs can be studied using MD simulations. For example, the implication of powder bed fusion process thermal conditions on the mechanical characteristics of Cantor alloys was studied in the work [34]. The authors varied the laser scan speed, laser power, and unidirectional and reversing laser passes in a wide range during the MD simulations to adjust the conditions to produce HEAs with the desired characteristics. The MD method is widely used for the investigation of the mechanical properties of HEAs, for example, cyclic plasticity [35]. This method allows considering the influence of the temperature and twin boundaries on the features of the structure formation of the CoCrFeMnNi HEA. However, for studying large systems of atoms with comparably high accuracy, it is important to choose the correct modelling parameters [36].

One of the main features of Cantor HEAs is their high impact strength, which reaches a value of 230 kJ/m² at a temperature of 77 K, which is much higher than that of conventional alloys [37]. In works [38,39], atomistic studies were carried out for the CoCrFeMnNi alloy. The authors observed the ductile behavior of this Cantor under tension at cryogenic temperatures. It was revealed that the plastic deformation scenario is determined by the

contribution of several components such as the transformation of the FCC lattice into the HCP martensite and the twinning and plasticity of GBs. The deformation of the Cantor CoCrFeMnNi alloy at low temperatures proceeds with the transformation of the crystalline phase into an amorphous one, which is accompanied by the formation of the so-called “amorphous bridge” leading to a separation of the cavities from the center of the crack origin [39,40]. This amorphization in the alloy occurs as a result of the formation of multi-dislocation compounds. The deformation mechanisms in these areas include partial dislocations of high-density Shockley, shear bands, and amorphous bridges, which are rarely found in conventional alloys at low temperatures. A detailed study on the effect of doping and diffusion processes at different temperatures on the evolution of HEAs' structures under various conditions is important for their mechanical design. Because of the compositional complexity of HEAs, there is a lack of clarity in current experimental and analytical studies regarding the effects of GB segregation on the deformation mechanisms of HEAs. For example, in some HEAs, GB segregation can lead to the formation of a “soft skin” region at the boundaries, where the atoms are less strongly bound and, therefore, more easily deformable. This can lead to enhanced plasticity and ductility, which can be beneficial for some applications [41]. On the other hand, GB segregation can also lead to the formation of brittle phases or precipitates, which can cause cracking or fracture under stress. In some cases, GB segregation can also influence the deformation mode of the material. For example, in a nanocrystalline HEA, GB segregation can promote deformation through grain boundary sliding rather than dislocation motion [42].

Overall, the effect of GB segregation on the deformation mechanisms of HEAs depends on a variety of factors, including the specific alloy composition, processing conditions, and the nature of the segregation itself [43]. Understanding the underlying mechanisms of GB segregation formation and their impact on the mechanical properties is an active area of research in the field of HEAs. In this regard, this work aims to study the effect of GB segregations on the shear and tensile deformation behavior of equiatomic nanoscale CoCrCuFeNi HEA at room (300 K) and cryogenic (100 K) temperatures. The elemental GB segregation of each element type in the HEAs is considered. The mechanical characteristics of the nanoscale CoCrCuFeNi HEA with and without segregations are compared.

2. Simulation Details

The formation of GB segregations in metallic alloys is often observed during their solidification when they are cooled down from a high temperature and then held at a lower temperature [44]. However, due to limited spatial and temporal scales in atomistic simulations, it is difficult to capture the diffusion process in HEAs. The deformation mechanisms and effect of GB segregation in polycrystals are most appropriately studied using MD simulations for specific flat GBs with a certain geometry. Accordingly, in the current work, MD simulations of the shear deformation and stretching of the nanoscale CoCrCuFeNi HEA were carried out using bicrystals with tilt GBs.

The MD simulations were implemented with the Large-Scale Atomic/Molecular Massively Parallel Simulator (LAMMPS) software [45]. The visualization of the results was performed using Open Visualization Tools (OVITO) [46]. The CoCrCuFeNi HEA with a face-centered cubic structure was selected as the material of study [47]. Initially, the single-crystal model with orientations of [11-2], [111], [1-10] along the axes X, Y and Z, respectively, was created. Then, the bicrystal was obtained by rotating the upper and lower parts of the single crystal along the Z axis by $\pm 15^\circ$, respectively (Figure 1a). Thus, the misorientation between the formed grains was set to be 30° . We set a misorientation of 30° between grains to form a general high-angle GB. Solute atoms more readily form GB segregations at high-angle GBs rather than at low-angle GBs or special GBs with lower GB energy and free volume [43]. The dimensions of the created bicrystal were 17.6, 23.0, and 4.6 nm along the three orthogonal directions. The considered bicrystal model consisted of 156,000 atoms.

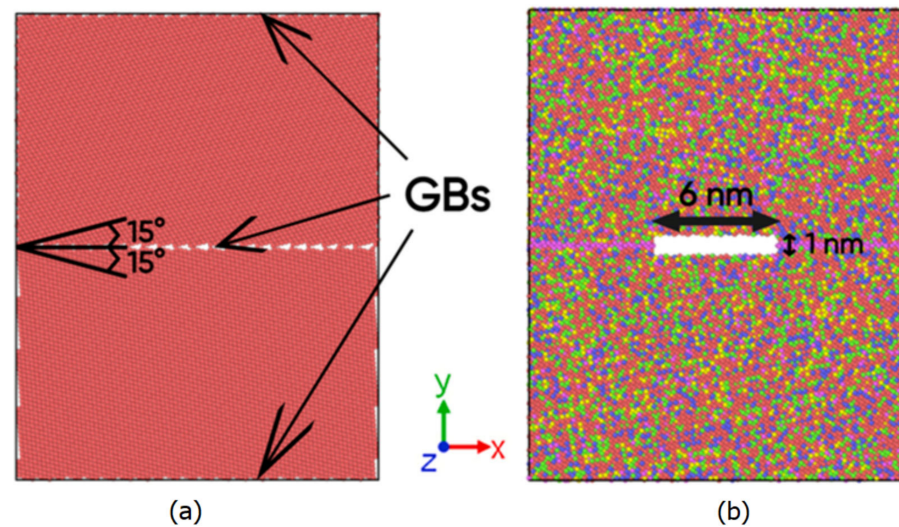


Figure 1. (a) The computational cell used for the simulations. (b) The bicrystal with the GB segregation of copper (colored in purple) and a crack in the middle of the GB.

The embedded-atom-method potential developed by Farkas D. and Carry A. [48] was used for the modelling. The integration of the atomic motion equations was carried out by the 4th-order extrapolation scheme with the Verlet method. A timestep of 1 fs was set. The initial samples were subjected to energy minimization with the conjugate gradient method by iteratively adjusting the atom coordinates and were further equilibrated at the considered deformation temperature. The minimization convergence criterion for the energy is 10^{-8} eV and for the force is 10^{-10} eV/Å. The structure optimization and subsequent deformation were modelled in the thermodynamic ensemble NPT (constant number of atoms in the simulation cell, as well as constant pressure and temperature) to control certain stress components at zero and maintain a constant temperature. The simulations were conducted at temperatures of 100 K and 300 K. Periodic boundary conditions were applied in all three orthogonal directions of the simulation cell. The tensile and shear loading were applied at a constant rate of 10^{-8} s $^{-1}$. Such a high strain rate is acceptable [49,50], considering the limited temporal scale of MD simulations.

For analyzing the effect of GB segregation on the deformation behavior of the bicrystals under applied loading, the segregation of single element type (Co, Cr, Cu, Fe, and Ni) is introduced at the GB region. Thus, five different bicrystals were created depending on the type of the GB segregation. The thickness of the segregated layer was set to 1, 3, or 5 Å. For the HEAs subject to the tension, a rectangular crack was additionally introduced into the middle of the GB of the bicrystals (Figure 1b). During the shear deformation, all stress components, except σ_{xy} , were kept equal to zero, while for the tensile deformation, all the components except σ_{yy} were controlled to be zero. The results for the bicrystals with GB segregation were compared with those obtained for the case without any GB segregation.

3. Results and Discussion

3.1. Shear Deformation

The material can reveal different deformation behavior when subjected to shear deformation depending on the presence of segregations that can lead to localized stress concentrations and deformation heterogeneities. Figure 2a shows the stress–strain curves obtained for the considered bicrystals after subjected to the shear deformation at 300 K.

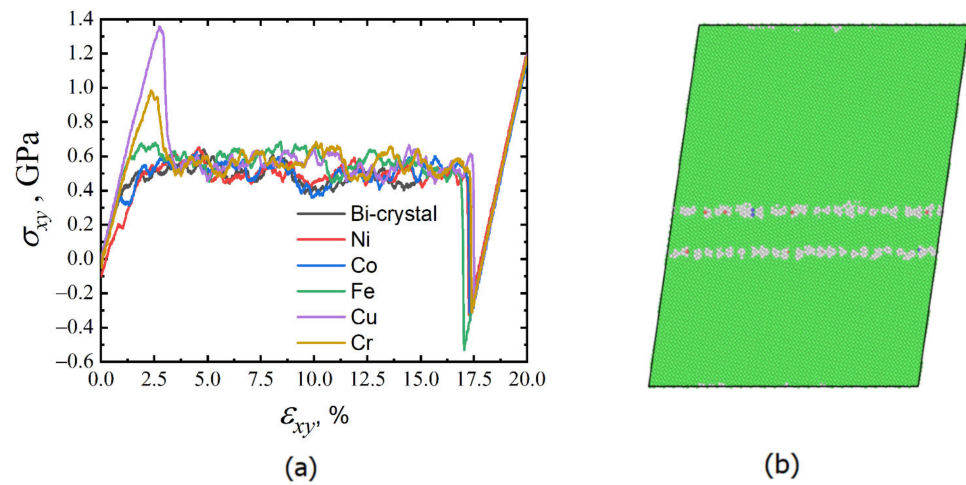


Figure 2. (a) The shear stress–strain curves for the considered bicrystals. The corresponding type of segregated element is indicated in the legend for each bicrystal, while the case without GB segregation is denoted as Bicrystal. (b) Structure of the bicrystal with GB segregation of Cr at 12% shear deformation.

It is revealed that the segregation of copper and chromium at the GB had a noticeable strengthening effect on the nanoscale CoCrCuFeNi HEA. The shear yield strength increased by 2 and 1.5 times, respectively, compared to the segregation-free bicrystal. The segregations of nickel, cobalt, and iron increased the strength insignificantly. The drop in the shear stress with further shear loading was associated with the plastic flow and structure relaxation through the GB migration (Figure 2b). Unlike the bicrystal without the GB segregation, for the other bicrystals, the middle GB with segregation remained stable, while the second GB, without segregation, moved towards the middle one. In Figure 2a, the sharp decrease in shear stress down to negative values at 17% shear strain and its subsequent linear growth were due to the GBs approaching each other, forming a single crystal (Figure 2b). The subsequent linear growth of the shear stress is explained by the strengthening of the single crystal as a result of elastic deformation.

3.2. The Effect of Segregation Layer Thickness

In addition, to investigate the effect of segregation on the strength of the bicrystal under study, the impact of the thickness of the segregated layer was also examined. Specifically, three different variants of chromium segregation with the thickness values of 1 Å, 3 Å, and 5 Å were considered, and the simulation results are presented in Figure 3.

Figure 3 shows that a higher stress level was required to move the GB as the thickness of the layer increased. An increase in the segregation thickness by 3 times caused the maximum shear stress to increase by 1.5 times, while a 5-fold increase in the thickness of the segregated layer resulted in a 2-fold increase in the maximum shear stress for chromium segregation. However, based on the relationships depicted in Figures 2a and 3, it can be inferred that the formation of a single crystal through the merging of two GBs was independent of both the thickness of the segregated layer and the type of segregated element.

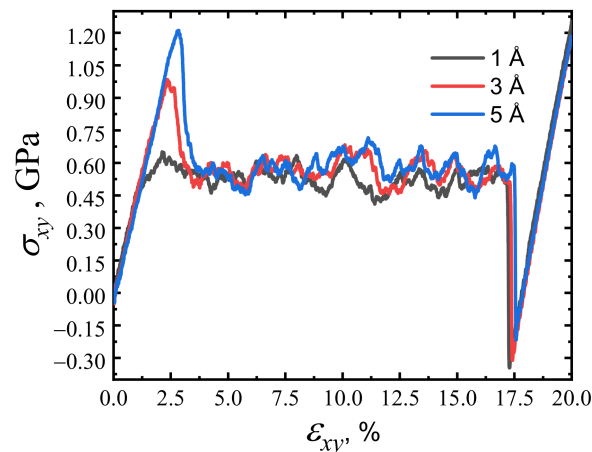


Figure 3. The shear stress–strain curves for the bicrystals with Cr segregation at GB. The corresponding thickness of the segregated layer (1, 3 or 5 Å) is indicated in the legend. The considered temperature is 300 K.

3.3. Tensile Deformation

Furthermore, modeling the nanoscale CoCrCuFeNi HEA stretching process and the effect of segregation on its mechanical properties were considered. The thickness of the segregated layer was 3 Å. The tensile deformation was carried out for a strain value of 15%.

Figure 4 shows the dependence of the tensile stress on the magnitude of the applied deformation. The evolution of the structure during the application of the load was accompanied by twinning sharp stress jumps corresponding to the restructuring of the bicrystal structure due to twins. In addition to the twins, the migration of GB near the crack contributed to the development of the deformed structure. The structure with copper segregation with the crack introduced breaks at 4.5% strain, demonstrating the smallest plasticity values within all considered cases. The configurations with nickel and chromium crack + segregation combinations revealed higher plasticity. In these cases, the breaks occurs when the lattice is being deformed to 8.7% and 13.5%, respectively. Nevertheless, the segregation of iron and cobalt and the configuration where the crack was introduced in the initial structure revealed the highest plasticity levels, reaching 15% and above.

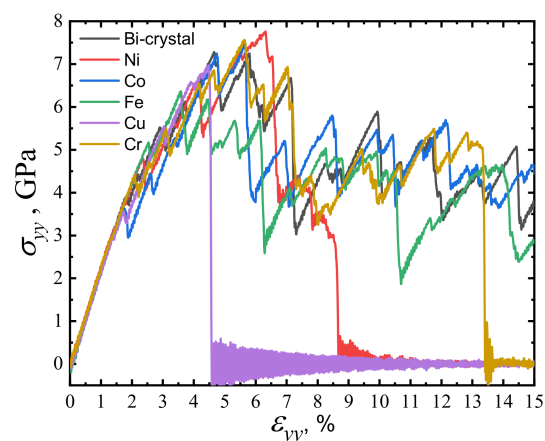


Figure 4. The tensile stress–strain curves for the considered bicrystals. The corresponding type of segregated element is indicated in the legend for each bicrystal, while the case without GB segregation is labeled as Bicrystal. The stress drop to zero corresponds to a break in the bicrystal. The considered temperature is 300 K.

Figure 5 shows the bicrystal structure with chromium segregation before the break. The common neighbor analysis (CNA) method is used to display structural defects. Amorphous

bridges [39,40] are clearly visible, which restrain the growing crack and lead to an increase in the plasticity of the bicrystal. The presence of disordered structure (grey area) near the crack indicates that the GBs slide and migrate. The twins are caused by the distortion of the crystal lattice under deformation slide and move throughout the bicrystal. For a more detailed study of mechanical properties under tension, the thickness of segregated layer was increased from 3 Å to 5 Å. In addition, the structure was deformed by up to 30%.

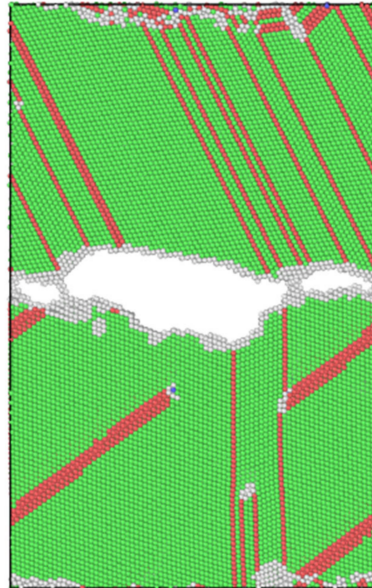


Figure 5. Bicrystal with chromium segregation at 12% strain. Twins are shown in red. Atoms of the disordered structure are shown in grey.

As can be seen from Figure 6, the bicrystal without segregation had the greatest plasticity—it broke when deformed by 16%. The segregation of nickel, cobalt, and iron reduced the plasticity of the bicrystal by 3–5%. The greatest decrease in plasticity was demonstrated by the bicrystals with copper and chromium segregation, the destruction of which occurred when they were stretched by up to 8%. Upon analyzing the dependencies presented in Figures 4 and 6, it was discovered that increasing the thickness of copper and nickel segregations led to a rise in the plasticity of the bicrystal. On the other hand, an increase in the thickness of chromium segregations reduced the plasticity of the bicrystal. Thus, it can be inferred that the strength characteristics of the bicrystal will increase when the thickness of the chromium-segregated layer at the middle GB is increased. This conclusion is in good agreement with the findings in Figure 3, where an increase in the thickness of the segregated layer of chromium resulted in an increase in the maximum shear stress.

Figure 7 shows the considered cells of the bicrystals in the process of stretching, before the structures broke. The atoms are colored according to CNA. As mentioned above, structures with the segregation of iron, nickel, and cobalt, as well as a bicrystal without segregation, had the greatest plasticity. These structures have a large number of twin defects. As can be seen from Figure 7f, the bicrystal without segregation had structural defects only in the upper half of the bicrystal's cell, but the spatial arrangement of the twins did not affect the deformation mechanism, since the twins actively migrated when the crystal lattice was distorted.

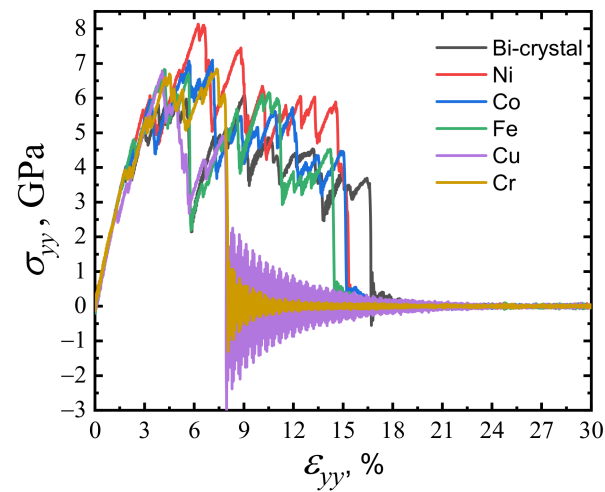


Figure 6. The tensile stress–strain curves for the considered bicrystals. The corresponding type of segregated element is indicated in the legend for each bicrystal, while the case without GB segregation is denoted as Bicrystal. The stress drop to zero corresponds to a break in the bicrystal. The considered temperature is 300 K.

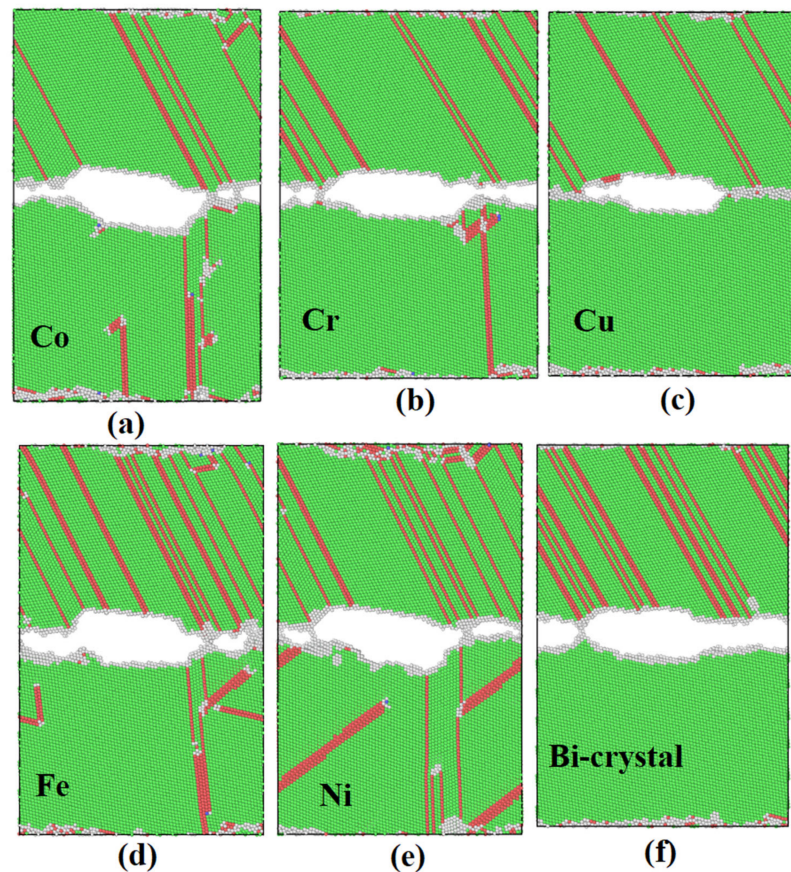


Figure 7. Bicrystals during stretching before breaking. Twins are shown in red, and atoms of the disordered structure are shown in grey. The figure shows the bicrystal with cobalt segregation (a), chromium segregation (b), copper segregation (c), iron segregation (d), and nickel segregation (e), and bicrystal without segregations (f).

The bicrystal with copper segregation at the GB broke almost along a straight line (Figure 7c). A detailed examination of the bicrystal under the strain shows that there were

no amorphous bridges formed next to the crack, which suggests an increase in the plasticity of the bicrystal. The bicrystal with the chromium segregation broke in the same way; however, we can observe small amorphous bridges along the X axis close to the edge of the crack (Figure 7b). The cases of cobalt, nickel, and iron segregations were characterized by a large number of atoms of the disordered structure around the crack. Therefore, we can observe several amorphous bridges that restrained the development of the main crack (Figure 7a,d,e). The structure without segregation had a plasticity level similar to the bicrystal with nickel or cobalt segregations; however, the mechanism of deformation, in that case, was different. The segregated atoms strongly distorted the crystal lattice during the deformation, thereby contributing to the formation of amorphous bridges. In the absence of segregation, fracture resistance occurred only due to chemical bonds existing between the phases of the bicrystal (Figure 7f).

The study did not reveal the specifics of the twin structure formation, which is dependent on the type of deformation, temperature, and thickness of the segregated layer. However, it is possible to gain a better understanding of this process by analyzing the deformation process with different ranges of element concentrations. These concentrations can be obtained through methods such as high cooling rates or doping.

By controlling the design of HEAs, the required mechanical properties can be achieved, depending on their intended application. It is important to note that the impact of doping elements on the alloy characteristics should be studied separately, as doping can lead to the formation of various phases with reduced physical and mechanical properties.

3.4. Deformation at 100 K

It is worth noting that modeling at 100 K did not reveal significant differences in the dynamics of the deformation-induced evolution of the structure compared to that at 300 K, as demonstrated in Figures 6 and 8. The primary distinction lies in the fact that at 100 K, the bicrystal containing copper segregation exhibited weaker plastic properties than at 300 K. The decrease in temperature from 300 K to 100 K caused the elongation of the bicrystal to drop by 3% before breaking. However, the deformation mechanism of the bicrystal in the presence of other types of atoms at GB segregation remained similar at both temperatures.

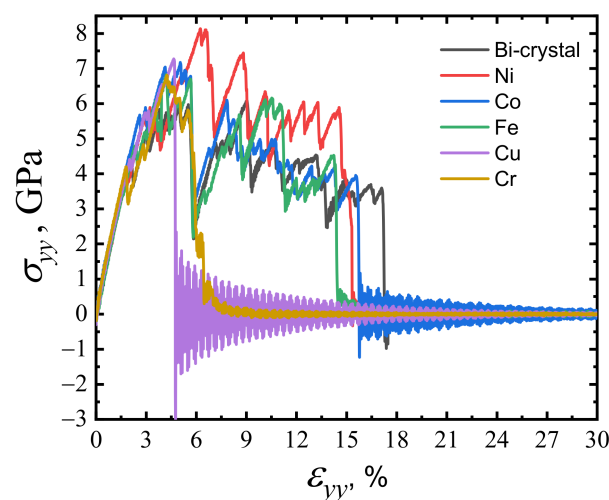


Figure 8. The tensile stress–strain curves for the considered bicrystals. The corresponding type of segregated element is indicated in the legend for each bicrystal, while the case without GB segregation is denoted as Bicrystal. The stress drop to zero corresponds to a break in the bicrystal. The considered temperature is 100 K. The thickness of the segregated layer is 5 Å.

4. Conclusions

In this study, we investigated the influence of segregations on the mechanical properties of an equiatomic nanoscale CoCrCuFeNi HEA using its bicrystal model. The results

demonstrate that GBs with segregations are unstable and relocate under shear deformation, with the presence of a segregated layer fixing one of the GBs. During deformation, the structure evolves due to the formation and migration of twins and the migration of GBs in the vicinity of the crack. The bicrystal with copper and chromium segregations exhibited the highest strength under shear deformation, and the maximum shear stress increased with an increase in the thickness of the segregation layer. Conversely, the bicrystal without segregation had the greatest plasticity. An increase in the thickness of the segregated layer from 3 Å to 5 Å in the bicrystal with the crack led to a decrease in its plasticity. Additionally, an increase in strength during stretching was observed for the bicrystal with chromium segregation, while an increase in the thickness of nickel and copper segregations at the GB of the bicrystal made it more ductile. The simulation results indicate that the mechanical properties of the studied bicrystal are similar at both 300 K and a cryogenic temperature of 100 K. Only a slight decrease in plasticity was observed at 100 K for the bicrystal containing the copper segregation. Future studies are required to investigate the contribution of cryogenic temperature to the formation of amorphous bridges with a higher number of segregations. Additionally, the impact of misorientation between GBs in the CoCrCuFeNi HEA containing cracks near the GBs on its mechanical properties is an important aspect that requires further investigation.

Overall, our results provide important insights into the correlation between the structure and properties of new types of the nanoscale CoCrCuFeNi HEA demonstrating the potential to control the mechanical properties of HEAs through the manipulation of the thickness and type of segregations. Despite many experimental studies on the deformation behavior of various HEAs, to the best of our knowledge, there are few experimental results reporting on the influence of segregations at GBs on deformation mechanisms specifically in the CoCrCuFeNi HEA. Therefore, our results cannot be directly compared with experimental ones. However, the GB segregation of Cr in HEAs and its positive effect were discussed earlier in [51]. The authors reported that Cr has a strong self-bonding tendency leading to improved GB strength. Moreover, the strengthening effect of Cu atoms at the GBs of CoCrCuFeNi HEA was observed earlier in [52] using combined MD/Monte Carlo modelling. Similarly, we observed higher stress required for the plastic shear deformation of bicrystals with Cr and Cu at GBs compared with other cases. We believe that this study can be helpful for a better understanding of the effect of various GB segregations on the mechanical properties of HEAs. However, it should be noted that the impact of doping elements on HEAs' characteristics requires further deep investigations, as doping may lead to the formation of various phases with reduced physical and mechanical properties.

Author Contributions: Conceptualization, E.A.K. and R.I.B.; methodology, A.M.K.; software, A.M.K. and A.V.Y.; data curation, A.A.K.; writing—original draft preparation, A.M.K.; writing—review and editing, E.A.K.; visualization, E.Z.K.; supervision, E.A.K. All authors have read and agreed to the published version of the manuscript.

Funding: The research was carried out with financial support from the Ministry of Science and Higher Education of the Russian Federation within the framework of the state assignment of the Ufa University of Science and Technology (Agreement No. 075-03-2023-119) for the Youth Research Laboratory of the Center for Metals and Alloys under Extreme Conditions for K.A.M., grant NSH-4320.2022.1.2 for K.A.A., and grant RSF 21-12-00275 for K.E.A.

Institutional Review Board Statement: Not applicable.

Informed Consent Statement: Not applicable.

Data Availability Statement: The datasets are available from the authors upon reasonable request (arseny.m.kazakov@gmail.com).

Conflicts of Interest: The authors declare no conflict of interest.

References

1. Crismaru, I.V.; Dragomir-Stanciu, D.; Atanasiu, M.V.; Pintilei, G.L. The Behavior of a 1.4301 Stainless Steel Subjected to Cryogenic Temperatures. *Procedia Technol.* **2015**, *19*, 247–253. [\[CrossRef\]](#)
2. Guo, X.; Zhang, K.; Liu, J.; Li, Y.; Zuo, X.; Xiao, H.; He, G. Tensile deformation mechanism of Sn-37Pb solder alloy at cryogenic temperatures. In Proceedings of the 2021 22nd International Conference on Electronic Packaging Technology (ICEPT), Xiamen, China, 14–17 September 2021; pp. 1–4.
3. Yeh, J.-W.; Chen, S.K.; Lin, S.-J.; Gan, J.-Y.; Chin, T.-S.; Shun, T.-T.; Tsau, C.-H.; Chang, S.-Y. Nanostructured High-Entropy Alloys with Multiple Principal Elements: Novel Alloy Design Concepts and Outcomes. *Adv. Eng. Mater.* **2004**, *6*, 299–303. [\[CrossRef\]](#)
4. George, E.P.; Curtin, W.A.; Tasan, C.C. High entropy alloys: A focused review of mechanical properties and deformation mechanisms. *Acta Mater.* **2020**, *188*, 435–474. [\[CrossRef\]](#)
5. Cantor, B.; Chang, I.T.H.; Knight, P.; Vincent, A.J.B. Microstructural development in equiatomic multicomponent alloys. *Mater. Sci. Eng. A* **2004**, *375–377*, 213–218. [\[CrossRef\]](#)
6. Senkov, O.N.; Scott, J.M.; Senkova, S.V.; Meisenkothen, F.; Miracle, D.B.; Woodward, C.F. Microstructure and elevated temperature properties of a refractory TaNbHfZrTi alloy. *J. Mater. Sci.* **2012**, *47*, 4062–4074. [\[CrossRef\]](#)
7. Singh, S.; Wanderka, N.; Murty, B.S.; Glatzel, U.; Banhart, J. Decomposition in multi-component AlCoCrCuFeNi high-entropy alloy. *Acta Mater.* **2011**, *59*, 182–190. [\[CrossRef\]](#)
8. Tang, W.Y.; Yeh, J.W. Effect of Aluminum Content on Plasma-Nitrided Al × CoCrCuFeNi High-Entropy Alloys. *Metall. Mater. Trans. A* **2009**, *40*, 1479–1486. [\[CrossRef\]](#)
9. Ren, B.; Liu, Z.X.; Li, D.M.; Shi, L.; Cai, B.; Wang, M.X. Effect of elemental interaction on microstructure of CuCrFeNiMn high entropy alloy system. *J. Alloys Compd.* **2010**, *493*, 148–153. [\[CrossRef\]](#)
10. Varalakshmi, S.; Rao, G.A.; Kamaraj, M.; Murty, B.S. Hot consolidation and mechanical properties of nanocrystalline equiatomic AlFeTiCrZnCu high entropy alloy after mechanical alloying. *J. Mater. Sci.* **2010**, *45*, 5158–5163. [\[CrossRef\]](#)
11. Qiu, X.W.; Zhang, Y.P.; He, L.; Liu, C. Microstructure and corrosion resistance of AlCrFeCuCo high entropy alloy. *J. Alloys Compd.* **2013**, *549*, 195–199. [\[CrossRef\]](#)
12. Tong, Y.; Chen, D.; Han, B.; Wang, J.; Feng, R.; Yang, T.; Zhao, C.; Zhao, Y.; Guo, W.; Shimizu, Y.; et al. Outstanding tensile properties of a precipitation-strengthened FeCoNiCrTi0.2 high-entropy alloy at room and cryogenic temperatures. *Acta Mater.* **2019**, *165*, 228–240. [\[CrossRef\]](#)
13. Wei, C.; Lu, Y.; Du, X.; Li, T.; Wang, T.; Liaw, P.K. Remarkable strength of a non-equiatomic Co₂₉Cr₂₉Fe₂₉Ni_{12.5}W_{0.5} high-entropy alloy at cryogenic temperatures. *Mater. Sci. Eng. A* **2021**, *818*, 141446. [\[CrossRef\]](#)
14. Hu, Y.J. First-principles approaches and models for crystal defect energetics in metallic alloys. *Comput. Mater. Sci.* **2023**, *216*, 111831. [\[CrossRef\]](#)
15. Wu, D.; Shuang, S.; Liang, Y.; Tian, X.; Kang, G.; Zhang, X. Interactions between screw dislocation and twin boundary in high-entropy alloy: A molecular dynamic study. *Comput. Mater. Sci.* **2022**, *213*, 111626. [\[CrossRef\]](#)
16. Tsuchiya, T.; Tsuchiya, J.; Dekura, H.; Ritterbex, S. Ab Initio Study on the Lower Mantle Minerals. *Annu. Rev. Earth Planet Sci.* **2020**, *48*, 99–119. [\[CrossRef\]](#)
17. Dittler, E.; Lubert, S. Vibrational spectroscopy by means of first-principles molecular dynamics simulations. *Wiley Interdiscip. Rev. Comput. Mol. Sci.* **2022**, *12*, e1605. [\[CrossRef\]](#)
18. Hao, L.Y.; Wen, X.Z.; Lei, X.W.; Yao, W.J.; Wang, N. Distinct nitriding behaviors of γ and γ' phases in Ni-based superalloys: A first-principles study. *J. Alloys Compd.* **2022**, *920*, 165996. [\[CrossRef\]](#)
19. Tang, Y.; Li, W.; Li, C.; Lu, S.; Vitos, L.; Pyczak, F. First-Principles Calculations of Elastic and Thermodynamic Properties for Multi-component Co-based Superalloys. *Metall. Mater. Trans. A* **2022**. [\[CrossRef\]](#)
20. Aravindh, S.A.; Kistanov, A.A.; Alatalo, M.; Kömi, J.; Huttula, M.; Cao, W. Incorporation of Si atoms into CrCoNiFe high-entropy alloy: A DFT study. *J. Phys. Condens. Matter* **2021**, *33*, 135703. [\[CrossRef\]](#) [\[PubMed\]](#)
21. Cui, H.; Tan, Y.; Bai, R.; Li, Y.; Zhao, L.; Zhuang, X.; Wang, Y.; Chen, Z.; Li, P.; You, X.; et al. Effect of melt superheat treatment on solidification behavior and microstructure of new Ni–Co based superalloy. *J. Mater. Res. Technol.* **2021**, *15*, 4970–4980. [\[CrossRef\]](#)
22. Miura, A.; Osada, T.; Kawagishi, K.; Uchida, K. Thermal transport properties of Ni–Co-based superalloy. *AIP Adv.* **2020**, *10*, 125118. [\[CrossRef\]](#)
23. Lian, Y.; Wang, X.; Gao, L.; Yin, Q.; Hu, P.; Wen, Z.; Wang, J. Microstructure and Tensile Behavior of a Novel Monocrystalline Co-Based Superalloy at Different Temperatures. *Adv. Eng. Mater.* **2022**, *24*, 2101037. [\[CrossRef\]](#)
24. Korznikova, E.A.; Shunaev, V.V.; Shepelev, I.A.; Glukhova, O.E.; Dmitriev, S.V. Ab initio study of the propagation of a supersonic 2-crowdion in fcc Al. *Comput. Mater. Sci.* **2022**, *204*, 111125. [\[CrossRef\]](#)
25. Shepelev, I.A.; Bayazitov, A.M.; Korznikova, E.A. Modeling of supersonic crowdion clusters in FCC lattice: Effect of the interatomic potential. *J. Micromechanics Mol. Phys.* **2021**, *6*, 2050019. [\[CrossRef\]](#)
26. Kolesnikov, I.D.; Shepelev, I.A. Excitation and propagation of 1-crowdion in bcc niobium lattice. *Mater. Technol. Des.* **2022**, *4*, 5–10. [\[CrossRef\]](#)
27. Chetverikov, A.P.; Shepelev, I.A.; Korznikova, E.A.; Kistanov, A.A.; Dmitriev, S.V.; Velarde, M.G. Breathing subsonic crowdion in Morse lattices. *Comput. Condens. Matter* **2017**, *13*, 59–64. [\[CrossRef\]](#)
28. Shepelev, I.A.; Dmitriev, S.V.; Kudreyko, A.A.; Velarde, M.G.; Korznikova, E.A. Supersonic voidions in 2D Morse lattice. *Chaos Solit. Fractals* **2020**, *140*, 110217. [\[CrossRef\]](#)

29. Yankovskaya, U.I.; Zakharov, P.V. Heat resistance of a Pt crystal reinforced with CNT's. *Mater. Technol. Des.* **2021**, *3*, 64–67. [[CrossRef](#)]
30. Shepelev, I.A.; Chetverikov, A.P.; Dmitriev, S.V.; Korznikova, E.A. Shock waves in graphene and boron nitride. *Comput. Mater. Sci.* **2020**, *177*, 109549. [[CrossRef](#)]
31. Korznikova, E.A.; Rysaeva, L.K.; Savin, A.V.; Soboleva, E.G.; Ekomasov, E.G.; Ilgamov, M.A.; Dmitriev, S.V. Chain Model for Carbon Nanotube Bundle under Plane Strain Conditions. *Materials* **2019**, *12*, 3951. [[CrossRef](#)] [[PubMed](#)]
32. Chen, H.Y.; Tsou, N.T. The Analysis of Thermal-Induced Phase Transformation and Microstructural Evolution in Ni-Ti Based Shape Memory Alloys by Molecular Dynamics. *Comput. Model. Eng. Sci.* **2019**, *120*, 319–332. [[CrossRef](#)]
33. Yoon, T.; Kang, S.; Kang, T.Y.; Kim, T.S. Detection of Graphene Cracks by Electromagnetic Induction, Insensitive to Doping Level. *Comput. Model. Eng. Sci.* **2019**, *120*, 351–361. [[CrossRef](#)]
34. Jamil, I.R.; Mustaquim, A.M.; Islam, M.; Hasan, M.N. Molecular dynamics perspective of the effects of laser thermal configurations on the dislocation and mechanical characteristics of FeNiCrCoCu HEA through powder bed fusion process. *Mater. Today Commun.* **2022**, *33*, 104998. [[CrossRef](#)]
35. Du, X.; Lu, X.; Shuang, S.; Wang, Z.; Xiong, Q.-L.; Kang, G.; Zhang, X. Cyclic Plasticity of CoCrFeMnNi High-Entropy Alloy (HEA): A Molecular Dynamics Simulation. *Int. J. Appl. Mech.* **2021**, *13*, 2150006. [[CrossRef](#)]
36. Lu, D.; Wang, H.; Chen, M.; Lin, L.; Car, R.; Weinan, E.; Jia, W.; Zhang, L. 86 PFLOPS Deep Potential Molecular Dynamics simulation of 100 million atoms with ab initio accuracy. *Comput. Phys. Commun.* **2021**, *259*, 107624. [[CrossRef](#)]
37. Gludovatz, B.; Hohenwarter, A.; Catoor, D.; Chang, E.H.; George, E.P.; Ritchie, R.O. A fracture-resistant high-entropy alloy for cryogenic applications. *Science* **2014**, *345*, 1153–1158. [[CrossRef](#)]
38. Ji, W.; Wu, M.S. Atomistic studies of ductile fracture of a single crystalline cantor alloy containing a crack at cryogenic temperatures. *Eng. Fract. Mech.* **2021**, *258*, 108120. [[CrossRef](#)]
39. Ji, W.; Wu, M.S. Nanoscale insights into the damage tolerance of Cantor alloys at cryogenic temperatures. *Int. J. Mech. Sci.* **2022**, *226*, 107406. [[CrossRef](#)]
40. Ji, W.; Wu, M.S. Nanoscale origin of the crystalline-to-amorphous phase transformation and damage tolerance of Cantor alloys at cryogenic temperatures. *Acta Mater.* **2022**, *226*, 117639. [[CrossRef](#)]
41. Luo, J.; Zhou, N. High-entropy grain boundaries. *Commun. Mater.* **2023**, *4*, 7. [[CrossRef](#)]
42. Zhou, N.; Hu, T.; Huang, J.; Luo, J. Stabilization of nanocrystalline alloys at high temperatures via utilizing high-entropy grain boundary complexions. *Scr. Mater.* **2016**, *124*, 160–163. [[CrossRef](#)]
43. Babicheva, R.; Jarlov, A.; Zheng, H.; Dmitriev, S.; Korznikova, E.; Nai, M.L.S.; Ramamurty, U.; Zhou, K. Effect of short-range ordering and grain boundary segregation on shear deformation of CoCrFeNi high-entropy alloys with Al addition. *Comput. Mater. Sci.* **2022**, *215*, 111762. [[CrossRef](#)]
44. Li, L.; Kamachali, R.D.; Li, Z.; Zhang, Z. Grain boundary energy effect on grain boundary segregation in an equiatomic high-entropy alloy. *Phys. Rev. Mater.* **2020**, *4*, 053603. [[CrossRef](#)]
45. Plimpton, S. Fast Parallel Algorithms for Short-Range Molecular Dynamics. *J. Comput. Phys.* **1995**, *117*, 1–19. [[CrossRef](#)]
46. Stukowski, A. Visualization and analysis of atomistic simulation data with OVITO—the Open Visualization Tool. *Model. Simul. Mater. Sci. Eng.* **2010**, *18*, 015012. [[CrossRef](#)]
47. Cantor, B. Multicomponent high-entropy Cantor alloys. *Prog. Mater. Sci.* **2021**, *120*, 100754. [[CrossRef](#)]
48. Farkas, D.; Caro, A. Model interatomic potentials and lattice strain in a high-entropy alloy. *J. Mater. Res.* **2018**, *33*, 3218–3225. [[CrossRef](#)]
49. Xiao, J.; Deng, C. Martensite transformation induced superplasticity and strengthening in single crystalline CoNiCrFeMn high entropy alloy nanowires: A molecular dynamics study. *Mater. Sci. Eng. A* **2020**, *793*, 139853. [[CrossRef](#)]
50. Jarlov, A.; Ji, W.; Zhu, Z.; Tian, Y.; Babicheva, R.; An, R.; Seet, H.L.; Nai, M.L.S.; Zhou, K. Molecular dynamics study on the strengthening mechanisms of Cr–Fe–Co–Ni high-entropy alloys based on the generalized stacking fault energy. *J. Alloys Compd.* **2022**, *905*, 164137. [[CrossRef](#)]
51. Li, Q.; Mo, J.; Ma, S.; Duan, F.; Zhao, Y.; Liu, S.; Liu, W.; Zhao, S.; Liu, C.; Liaw, P.; et al. Defeating hydrogen-induced grain-boundary embrittlement via triggering unusual interfacial segregation in FeCrCoNi-type high-entropy alloys. *Acta Mater.* **2022**, *241*, 118410. [[CrossRef](#)]
52. He, T.; Qi, Y.; Ji, Y.; Feng, M. Grain boundary segregation-induced strengthening-weakening transition and its ideal maximum strength in nanopolycrystalline FeNiCrCoCu high-entropy alloys. *Int. J. Mech. Sci.* **2023**, *238*, 107828. [[CrossRef](#)]

Disclaimer/Publisher's Note: The statements, opinions and data contained in all publications are solely those of the individual author(s) and contributor(s) and not of MDPI and/or the editor(s). MDPI and/or the editor(s) disclaim responsibility for any injury to people or property resulting from any ideas, methods, instructions or products referred to in the content.